One way of representing the size and shape of biomass particles in combustion modeling

Anna Trubetskaya[a,*], Gert Beckmann[b], Johan Wadenbäck[c], Jens Kai Holm[d], Sitaram P Velaga[e], Roman Weber[f]

[a]*Division of Energy Science, Luleå University of Technology, 97187 Luleå, Sweden*
[b]*Retsch GmbH, Retsch Allee 15, 42781 Haan, Germany*
[c]*Amager power plant, HOFOR A/S, Kraftværkvej 37, 2300 Copenhagen S, Denmark*
[d]*DONG Energy Thermal Power A/S, Nesa Alle 1, 2820 Gentofte, Denmark*
[e]*Department of Health Sciences, Luleå University of Technology, 97187 Luleå, Sweden*
[f]*Institute of Energy Processes Engineering and Fuel Technology, Clausthal University of Technology, 38678 Clausthal-Zellerfeld, Germany*

Abstract

This study aims to provide a geometrical description of biomass particles that can be used in combustion models. The particle size of wood and herbaceous biomass was compared using light microscope, 2D dynamic imaging, laser diffraction, sieve analysis and focused beam reflectance measurement. The results from light microscope and 2D dynamic imaging analysis were compared and it showed that the data on particle width, measured by these two techniques, were identical. Indeed, 2D dynamic imaging was found to be the most convenient particle characterization method, providing information on both the shape and the external surface area. Importantly, a way to quantify all three dimensions of biomass particles has been established. It was recommended to represent a biomass particle in combustion models as an infinite cylinder with the volume-to-surface ratio (V/A) measured using 2D dynamic

*Corresponding author. anna.trubetskaya@ltu.se

imaging.

Keywords: biomass, 2D dynamic imaging, FBRM, laser diffraction, sieving

---

Nomenclature

A	Particle surface area [m^2]
AR	Aspect ratio
b	Particle width [m]
c_p	Specific heat capacity [J (kg K)$^{-1}$]
d	Diameter [m]
f	Dimensionality factor
l	Particle length [m]
L	Chord length [m]
m	Number of size classes
M_i	Class midpoint [m]
N	Class number
n	Number of counts per size class
P	Perimeter of a particle projection [m]
Q_3	Cumulative particle distribution, based on volume [%]
$\overline{q_3}$	Histogram
q_3	Frequency particle distribution, based on volume [% mm^{-1}]
r	Particle radius [m]
r_1, r_2	Distances from the area center to the particle edges [m]
$SPHT$	Circularity (Sphericity)
$Symm$	Symmetry
T	Temperature [°C]
t	Time [s]
V	Volume [m^3]
w	Size class weight
x_{cmin}	Smallest maximal chord [m]

$x_{Fe\,max}$	Feret maximum diameter [m]	ρ	Density [kg m^{-3}]
$x_{Ma\,min}$	Martin minimum diameter [m]	**Subscripts**	
		e	Effective
Greek symbols		p	Particle
λ	Thermal conductivity [W (m K)$^{-1}$]	s	Solid phase
		total	Total

1. Introduction

Biomass firing is used for power generation and is considered an important step in the reduction of greenhouse gas emissions. Anthropogenic CO_2 emissions can be decreased by biomass co-firing due to the lower regeneration time of biomass compared to bituminous coal. Thus, CO_2 released with biofuels can be reconsumed faster by plants via photosynthesis than the time needed to regenerate coal. The milling process is a necessary step in suspension firing [1]. Size reduction improves fuel conversion processes because of the creation of larger reactive surface areas [2, 3]. Biomass is, due to its fibrous structure, difficult to mill. Since the heating value of biomass is lower than coal, more biomass has to be used in order to achieve the same power output [4, 5]. Increased energy input into biomass comminution affects the total efficiency of a power plant, and too large particles often cause problems with flame stability and burnout.

Fuel characterization plays an important role in combustion modeling [6–11]. The surface area and volume of the particle are important parameters

since they determine combustion rates and define residence time. Various biomass shapes result in different volume-to-surface area ratios, which are important parameters in describing heat and mass transfer processes. For a given volume, spheres represent the largest volume-to-surface area ratio of any shape, which makes an assumption of spherical particles in combustion modeling rather conservative. Particle size analysis methods that assume a constant (spherical) shape are inadequate for biomass since irregularly shaped particles are typical and most often present. Furthermore, a disagreement between particle size distributions obtained by many particle size measurement techniques has been observed [12]. Most particle analyzers use one geometrical parameter by assuming a spherical form. However, as the fuel particle shape becomes more complex, at least two parameters (width and length) are necessary to describe the particle size.

Despite numerous studies on biomass particles [7, 9–11, 13, 14], there is no consensus on how to represent a biomass particle in combustion models. The common way involves approximating of the particle shape to regular geometrical bodies (e.g. parallelepiped, cylinder, cubes, ellipsoids). In combustion models from Yang et al. [14] and Yin et al. [13], particles are represented by cylindrical and spherical shapes, whereas Thunman et al. [7] treat particles in a one-dimensional model as plates, cylinders and spheres representing non-spherical shapes. The accuracy of particle models depends on both correct size distribution and characterization of fuel inhomogeneity in terms of shape and structure. The objective of this study is twofold: (1) to provide a geometrical description of biomass particles that can be used in combustion model; (2) to make suggestions for the size and shape of biomass particles.

In this work, the biomass particles' size and shape are characterized by using both 2D dynamic imaging analysis and microscopy. 2D dynamic imaging results are compared with particle size data obtained using focused beam reflectance measurement, laser diffraction and sieving techniques.

2. Materials and methods

2.1. Raw material characterization

Table 1 lists samples which were used in the particle size and shape characterization study.

Table 1: Samples specification. The bulk density, ash (% dry basis) and moisture (% as received) content were determined for poplar, wheat straw and pulverized wood pellets. Samples were comminuted in the rotor- and Loesche roller mills. Prior to particle size and shape analysis, samples were collected using a rotorprobe and a micro-riffler.

Identifier	**Samples**		
	Poplar	**Pulverized wood pellets**	**Wheat straw**
mill type	Rotor mill	Loesche roller mill	Rotor mill
sampling method	Micro-riffler	Rotorprobe	Micro-riffler
bulk density, g cm^{-3}	1.4	1.3	1.4
ash, % dry basis	1.3	0.5	4.1
moisture, % as received	7.9	7.8	10

Wheat straw and wood pellets represent the fuel types which are commonly used for suspension fired combustion with 100 % biomass. It is a challenge to obtain high operational flexibility at power plants by application of a broad biofuel range. Therefore, poplar, which is among the fastest

growing trees in the world, was selected for this study [15]. The moisture content and bulk density were measured using standard methods described in EN ISO 18134-1:2015 and EN ISO 17828:2015. The ash content was determined using a standard ash test at 550°C, according to the procedure described in EN ISO 18122:2015. The 8 mm pellets, without additives or binding agents, were produced in Latvia (LatGran). The pellets were transported to Avedøre power plant and comminuted in the horizontal Loesche roller mill. Pulverized wood was sampled from the pipeline (running to the burners) through a side opening by using a rotorprobe. Pellets consisted of 10 % hardwood and 90 % softwood, and were produced from 70 % fine sawdust and 30 % coarse sawdust. A larger percentage of softwood contains Scots pine (Pinus sylvestris), Norway spruce (Picea abies) and European aspen (Populus tremula), whereas a smaller percentage of hardwood consists of birch (Betula spp) and alder (Alnus spp), according to the feedstock classification described in EN ISO 17225-1. The age of the roundwood with bark used for making pellets ranged from 15 to 95 years.

Poplar and wheat straw samples were milled in a ZM200 rotor mill (Retsch GmbH, Germany) whereas pellets were comminuted in a LM 23.2 D horizontal roller mill (Loesche GmbH, Germany). All samples were milled to < 0.5 mm. Biomass samples were sieved to the 0.71-1 mm particle size fraction. Under fast heating conditions, which are relevant to suspension firing, biomass particles with mean diameters < 0.425 mm may be considered as thermally thin based on the previous modeling results [16], while the intra-particle heat conduction in larger particles plays a key role in biomass devolatilization. The previous results also indicated that the larger wood

particles (0.85-1 mm) required more than 1 s in the wire-mesh and drop tube reactors at 1000°C for complete conversion [17]. Therefore, the large biomass particles were selected for the shape characterization study because particles of size > 0.7 mm can often cause problems with flame stability and burnout. Prior to the analysis, biomass samples were divided into equal (100 mg) fractions using a PT100 micro-riffler (Retsch GmbH, Germany).

2.2. Particle size and shape characterization

2D dynamic imaging analysis. The particle size and shape were measured using the CAMSIZER (Retsch GmbH, Germany), designed for the particle size range from 0.03 to 30 mm. Particle shadows (projected area) were captured by two cameras: a zoom camera, designed for the analysis of smaller particles, and a basic-camera that was able to detect larger particles. The particle projected area was determined using the CAMSIZER 6.3.10 software (Retsch GmbH, Germany) which evaluates the particle size from the captured images by calculating the three parameters shown in Figure 1.

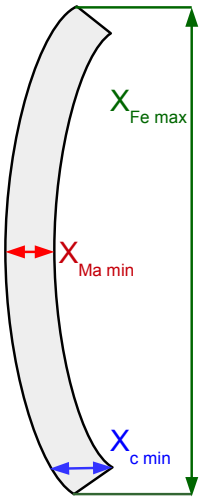

Figure 1: Martin minimal ($x_{Ma\,min}$), smallest maximal chord ($x_{c\,min}$) and Feret maximal ($x_{Fe\,max}$) diameters for a particle projection, as also shown in the Supplemental material.

The smallest maximal chord ($x_{c\,min}$) is defined as the smallest of all maximum chords of a particle projection. The Martin diameter is a characteristic length that divides the projected particle area into two equal halves [18]. The minimal Martin diameter ($x_{Ma\,min}$) is determined from the smallest Martin diameter of a particle projection [19]. The Feret diameter is a distance between two tangents placed perpendicular to the measurement direction [18]. The Feret maximal diameter is the longest Feret diameter of all measured Feret diameters of a particle projection [19]. The particle size distribution, based on the volume as shown in the Supplemental material, is represented by the $x_{Ma\,min}$ diameter. For the particle size analysis, a 100 mg sample was

used.

Shape characterization. In the present study, particle shape is characterized by both the sphericity (SPHT) and the aspect ratio (AR). Sphericity is one of the most commonly used parameters to express the deviation of a two-dimensional particle image from a sphere / circle and is defined as

$$SPHT = \frac{4 * \pi * A}{P^2}, \tag{1}$$

where P and A are the measured perimeter and area of a particle projection, respectively. A particle is considered to be spherical when sphericity is equal to 1, and non-spherical when it is less than 1. The aspect ratio is defined as the ratio of particle width ($b = x_{Ma\,min}$) to the particle length ($l = x_{Fe\,max}$) so that

$$AR = \frac{b}{l}. \tag{2}$$

Particle symmetry (Symm) is defined as

$$Symm = \frac{1}{2}\left(1 + \left(min\frac{r_1}{r_2}\right)\right), \tag{3}$$

where r_1 and r_2 are distances from the area center to the particle edges on the same line. The center (C) of area in Figure 2 is determined by the CAMSIZER software. Many lines are drawn so that each one passes through the area center between the particle's edges. The symmetry is calculated from the smallest ratio of the resulting segments (r_1 and r_2). For highly symmetrical particles like circles, ellipses or squares, the symmetry nears one. The center point divides each line in two parts. For asymmetrical particles (e.g. broken beads, triangles), the symmetry is less than one. The

symmetry varies from 0 to 0.5, and r_1 and r_2 overlap, if the center of the area is outside of a particle so that

$$\frac{r_1}{r_2} < 0. \tag{4}$$

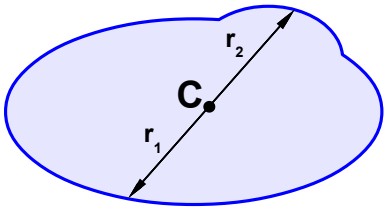

Figure 2: Definition of symmetry.

The symmetry is equal to 0.5, if the center of the area is exactly at the particle border.

Sieving. A vibrating AS 200 sieve shaker (Retsch GmbH, Germany) comprising seven sieves ranging from 0.25 to 4 mm in opening size and a bottom pan (< 0.25 mm) was used. The sieving analysis is described in EN ISO 17827-2:2016. Particles remaining on each sieve and in a bottom pan were collected and weighed using an electronic top pan balance (± 0.01 g accuracy). The cumulative retained undersize is the mass passed from the previous sieve, minus the mass retained on the current sieve [20]. Sieving was conducted for 15 min at 3 mm amplitude [21].

Particle size distribution. The results are presented as a cumulative particle size distribution, based on volume (Q_3). The cumulative particle size

distribution is described in EN ISO 9276-1:1998, and is defined as

$$Q_3(x_{Ma\,min,m}) = \sum_{i=1}^{m} \overline{q_3}(x_{Ma\,min,i})\Delta x_{Ma\,min,i}, \tag{5}$$

where $\overline{q_3}$ is the area of the histogram. The results of a particle size analysis are also presented as a frequency distribution over $x_{Ma\,min}$, based on volume (q_3), so that

$$q_3(x_{Ma\,min}) = \frac{dQ_3(x_{Ma\,min})}{dx_{Ma\,min}}. \tag{6}$$

The characteristic diameters, obtained from sieving and 2D dynamic imaging, were defined based on three sizes within the entire population: d10, d50, d90. The d50 value is the median particle size within the population, with 50 % of the population greater than this size, and 50 % smaller than this size. Similarly, 10 % of the population is smaller than the d10 size; while 90 % of the population is smaller than the d90 size [22]. All measurements were conducted in triplicate to establish repeatability which exceeded 95 % confidence intervals, as shown in the Supplemental material. The measurement inaccuracy from sieving analysis was mainly caused by weighing errors.

Light microscopy. Light microscopy of sawdust and disintegrated pellets was conducted using a 1750 microscope heating stage (Leica Microsystems, Germany) in order to characterize the particle shape. Digital images were captured using a camera attached to the microscope and then analyzed using the software that incorporates a simple ruler. The particle geometric parameters were measured manually using appropriate diameter definitions. At least 440 particles are required to obtain 10 particles in each fraction for statistically reliable results. In the microscopy analysis, about 500 biomass particles were

characterized. The width and length of a biomass particle were analyzed using a ruler in the microscope's software. Smaller particles were analyzed on a piece of adhesive tape. A single biomass particle was manually rotated by 90° in the sample plane to determine all three dimensions.

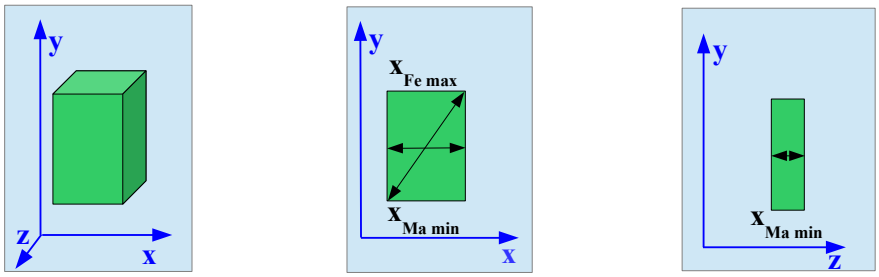

3(a): Biomass particle 3(b): Width and length 3(c): Thickness

Figure 3: Measurement of particle three dimensions (width, length, thickness) by the light microscopy.

Laser diffraction. The particle size distribution of biomass samples was determined by a 2000 particle size analyzer (Malvern Instruments Ltd, UK) using a wet method. The biomass samples were dispersed in ethanol. All measurements were made at room temperature and at 3200 rpm on at least two samples. The refractive indices of biomass and ethanol were taken as 1.53 and 1.33, respectively [23]. The Sauter mean diameter was calculated as the surface area moment mean, and defined as

$$D_{32} = \frac{\sum n_i d_i^3}{n_i d_i^2}. \tag{7}$$

The volume mean diameter (D_{43}) was calculated as follows

$$D_{43} = \frac{\sum n_i d_i^4}{n_i d_i^3}, \tag{8}$$

where n_i is the number of particles with measured diameter d_i.

Focused beam reflectance measurement. The particle size distribution was determined using a G400 focused beam reflectance analyzer (Mettler Toledo, UK). The focused beam of laser light scans across individual particles at a fixed scan speed [24]. The backscattered light is detected as a signal issued from one particle edge to an opposing edge. The pulse signal duration is multiplied by the scan speed to calculate the chord length.

A 1 g of biomass was added to a 200 ml glass beaker filled with methanol. The biomass particles were stirred using an anchor type stirrer at 200 rpm at room temperature. Five measurements, each of 15 min duration, were made on each sample, and the data was recorded using the FBRM acquisition software. The chord lengths, in the range of 1 to 1000 μm, were split into ninety classes (N = 90). The total number of counts per class (n_i) is determined as

$$n_{total} = \sum_{1}^{N} n_i. \tag{9}$$

The results of a particle size analysis by FBRM are always presented as an unweighted chord length distribution. For any particle shape, the number of small chord length counts statistically outweighs the large particle chord length counts [25]. The class weighting was used in order to emphasize the longer chords, which represent the most likely lengths of wood fibers. A class-specific weight (w_i) to the number of counts (n_i) is then used to calculate weighted chord length so that

$$L_i = w_i \cdot n_i. \tag{10}$$

The weights (w_i) are obtained from the class midpoint (M_i)

$$w_i = \frac{M_i^j}{\sum_{i=1}^{N} M_i^j} \cdot N. \tag{11}$$

In equation 11, j=0 and j=2 are unweighted and square-weighted particle size distributions, respectively. The raw chord length data (j=0) is first collected by the FBRM probe, and then weighted using the square-weighting function. The mean chord length on a square-weighted basis is calculated as

$$\bar{L} = \frac{\sum_{i=1}^{N} n_i M_i^3}{\sum_{i=1}^{N} n_i M_i^2}. \tag{12}$$

Similar to volume-weighted distributions, the square-weighted distributions are sensitive to the amount of large particles. The square-weighted mean chord length is equivalent to the Sauter mean diameter [26–28]. The results of a particle size analysis are presented as a square-weighted frequency distribution and calculated as

$$q_3(L) = \frac{n_i L_i^2}{\sum_{i=1}^{N} (n_i L_i^2)}. \tag{13}$$

The FBRM results of Heath et al. [27] showed that the square-weighting is effectively a cube (volume) weighting and is comparable to the volume-based distribution used in laser diffraction.

3. Results

3.1. Particle size analysis

Because of the coupling between chemistry and heat and mass transfer during particle conversion, fuel particle size has a noticeable effect on com-

bustion process characteristics. Thus, the choice of the suitable particle size descriptors is relevant. In 2D dynamic imaging, the minimal Martin diameter ($x_{Ma\,min}$) represents a particle width, which is larger than its thickness. The Feret maximal diameter, representing the length, is greater than the width. Therefore, the Martin minimal ($x_{Ma\,min}$) and Feret maximal ($x_{Fe\,max}$) diameters are suitable parameters to represent the width and length of biomass particles, confirming previous results of Trubetskaya et al. [29].

The most suitable descriptor of particle size, when characterized using sieving and 2D dynamic imaging, is the smallest maximal chord ($x_{c\,min}$) [19]. The difference between particle size distributions over $x_{Ma\,min}$ and $x_{c\,min}$ diameters is small as shown in Supplementary Figure S-5. Thus, the particle width can be represented by $x_{c\,min}$ diameter when the 2D dynamic imaging device is not available. Figure 4 shows particle size distributions for poplar, pulverized wood sample and wheat straw, characterized using the sieving, 2D dynamic imaging, laser diffraction and focused beam reflectance technique.

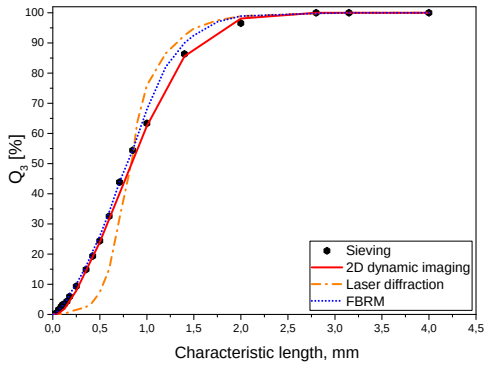

4(a): Poplar

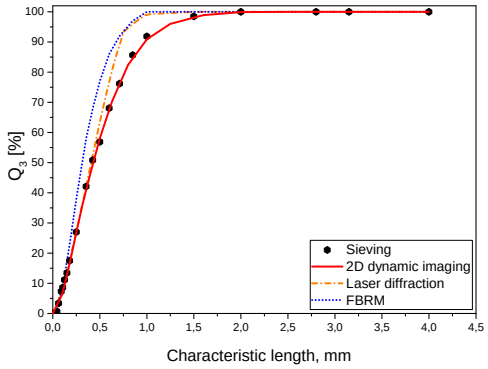

4(b): Pulverized wood

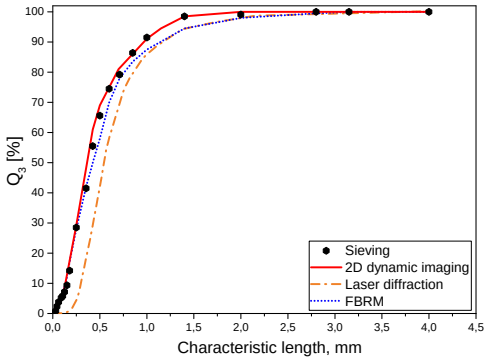

4(c): Wheat straw

Figure 4: Cumulative particle size distribution Q_3, based on volume, for poplar, pulverized wood and wheat straw samples characterized by the sieving, 2D dynamic imaging ($x_{Ma,min}$), laser diffraction and focused beam reflectance technique.

The data obtained by different particle size characterization techniques is repeatable, as shown in the Supplemental material. The particle size analysis indicated that pulverized wood contained a larger fraction of small particles compared to poplar and wheat straw. The poplar particle size distribution was more heterogeneous than those of other fuels. Figure 4 shows that sieving and 2D dynamic imaging produced very similar size distributions for all biomass samples, while a significant deviation was observed when compared with the results from the laser diffraction and the FBRM.

The 2D dynamic imaging captures the shadows of randomly orientated 3D particles. 2D projections of a 3D particle and their dependency on the orientation and shape can be recorded by CAMSIZER cameras in various ways. Gil et al. [30] reported that sieve size corresponds to biomass particle width (shorter dimension) with sieving efficiency around 70 % depending on the feedstock and considered size fraction. The square-shaped sieve apertures allow the passage of about 0.8 times the width of the particle [31]. During sieving, particles always fall through the sieves with their smallest two-dimensional projection, which does not appear the case for biomass particles. In 2D dynamic imaging of elongated biomass particles, the width of a particle projection does not change significantly, while the length of a particle is strongly influenced by the particle rotation / orientation in the measurement shaft. The $x_{Ma\,min}$ diameter does not change as extensively as the $x_{c\,min}$. The sieving curve was close to the 2D dynamic imaging curve representing $x_{Ma\,min}$ particle model for all samples. Overall, sieving is more convenient when a large biomass sample quantity has to be analyzed and when the particle size exceeds the measurement limitations of other sizing

techniques, while 2D dynamic imaging is recommended when information about particle shape is required.

Particle size distributions measured by 2D dynamic imaging deviate significantly from those obtained using the FBRM device. 2D dynamic imaging evaluates the particle size based on attributes of non-spherical shapes. The FBRM device measures chord lengths, where a chord length is defined as a straight line between any two points on the edge of a particle. The accuracy of particle size characterization using the FBRM device might be influenced by the various shapes of a biomass particle with broken edges. The results of the laser diffraction analysis showed that both poplar and wheat straw samples contained a larger fraction of course particles - a result which was not in agreement with other size characterization techniques. The difference between the particle size distributions measured by the laser diffraction and the other techniques is large. Since biomass particle shapes deviate significantly from a sphere, the spherical assumptions in the optical models are not valid. Thus, the results of the laser diffraction analysis do not characterize the real size of biomass particles. The discrepancy was partly due to the fact that the laser diffraction measures the diameters of equivalent volume particles from the diffraction signals [32–35]. The wrong assumption of random orientation of fibers in the laser diffraction affects measurement accuracy [32, 36].

3.2. Particle shape analysis

The particle shape was characterized using both the 2D dynamic imaging instrument and light microscopy. The small biomass particles of size $<$ 0.5 mm were more elongated (SPHT = 0.31 and aspect ratio AR = 0.11), as shown in Figure 5.

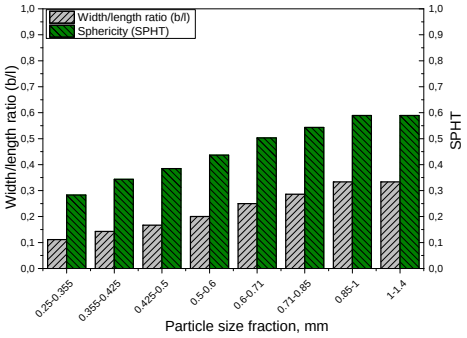

5(a): Poplar sphericity

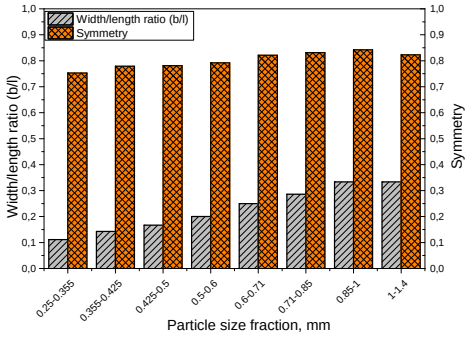

5(b): Poplar symmetry

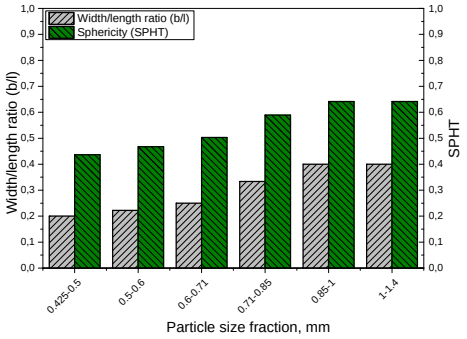

5(c): Pulverized wood sphericity

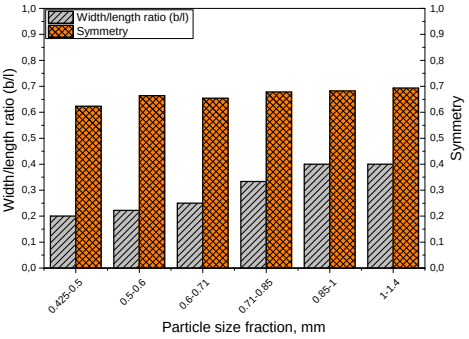

5(d): Pulverized wood symmetry

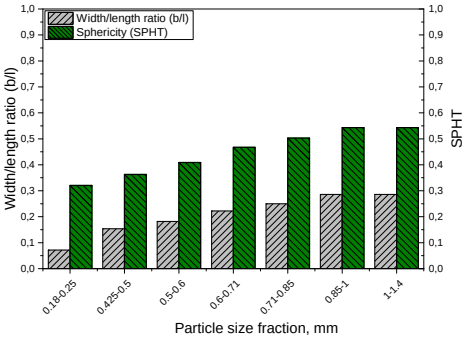

5(e): Wheat straw sphericity

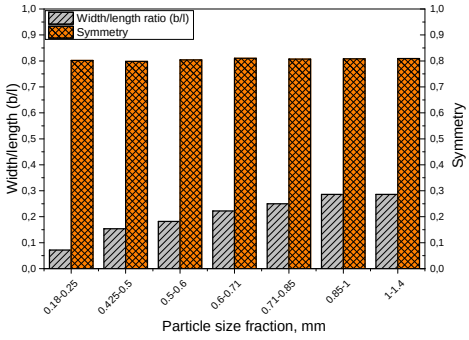

5(f): Wheat straw symmetry

Figure 5: Shape factors (sphericity/circularity and symmetry) in comparison to the aspect ratio (b/l) of poplar, pulverized wood and wheat straw samples which were sieved to the 0.71-1 mm fraction, and characterized by 2D dynamic imaging.

The aspect ratio of biomass particles measured by 2D dynamic imaging over $x_{Ma\,min}$ decreased from 0.25 to 0.11 with decreasing particle size, indicating that larger particles exhibited a more elongated shape. The sphericity (mean SPHT of all samples = 0.51) and the aspect ratio (mean AR of all samples = 0.32) for particle fractions > 0.5 mm indicate that they were more square-shaped. Symmetries of poplar and wheat straw particles were similar; particles were polygonal and symmetrical with holes (Symm = 0.8). Compared to the poplar and wheat straw samples, the pulverized wood showed a stronger anisotropy in shape (Symm = 0.68), which might be caused by the particle edge deformation during secondary comminution. Overall, 2D dynamic imaging analysis showed that the particles of a different size had similar rectangular shapes and that the ratio between particle dimensions did not change significantly with decreasing particle size, which is in line with the results of Cardoso et al. [37].

In Figure 6, the light microscopy results show elongated wheat straw particles. The main difference among the fuels was that the pulverized wood formed more square-shaped particles while the particles of poplar and wheat straw were elongated, confirming the results of 2D dynamic imaging in Figure 5. There was little change in the average particle shape among the size classes.

6(a): Poplar

6(b): Pulverized wood

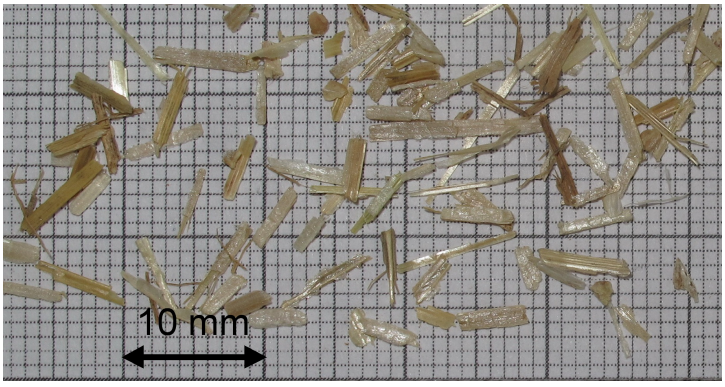

6(c): Wheat straw

Figure 6: Light microscopy images of (a) poplar, (b) pulverized wood and (c) wheat straw particles.

The major drawback of the 2D dynamic imaging is that two-dimensional projections can be generated only. Consequently, the third dimension cannot be obtained, and for the particle volume calculation, the thickness is often assumed to be equal to the width. In order to examine the accuracy of this simplification, the biomass particles were analyzed using 2D dynamic imaging and light microscopy. In terms of absolute accuracy, the microscopy provides a high resolution and high magnification images, but they only represent a small sample amount.

The 2D dynamic imaging results, together with the light microscopy data, are shown in Figure **??**. In the light microscopy analysis, $x_{Ma\,min}$ and $x_{Fe\,max}$ were determined manually to make the data from both techniques comparable. A significant difference was observed in particle length, represented by $x_{Fe\,max}$, while the deviations in the width, represented by $x_{Ma\,min}$, were almost negligible. The particle alignment has more influence on the measurement in 2D dynamic imaging. During the microscopy analysis, particles were aligned perpendicular to the measurement direction, and thus, the particle alignment only slightly influenced the particle size. The observation made by Igathinathane et al. [38] that the measured length depends on orientation angle in imaging analysis was confirmed in the present study. It was shown [38], that correction factors can rectify the overestimation. The microscopy and 2D dynamic imaging results with respect to $x_{Fe\,max}$ can be made comparable if the results from the imaging analysis are multiplied by $\cos(45°)$ [39], as shown in Supplementary Figure S-6.

Igathinathane et al. [38] used the $\sqrt{\pi}/2$ (≈ 0.886) correction factor to reduce the width and length of rectangular and cubic particles in imaging

analysis; the factor is close to the correction factor of $\cos(45°) \approx 0.707$. In 2D dynamic imaging software, the particle thickness is assumed to be equal to the width. The present microscopy results show that the particle thickness of woody and herbaceous feedstocks can be estimated to be 2/3 of the particle width ($x_{Ma\,min}$), as shown in Supplementary Figure S-7. The thickness of larger ($> 0.6\,\mathrm{mm}$) wheat straw and pulverized wood particles can be estimated as 1/2 of the particle's width, confirming the results of Momeni [40].

3.3. Representation of biomass particle shape in modeling

In suspension firing, biomass particles undergo rapid heating, drying and devolatization with the formation of char and volatiles. Devolatilization models often assume non-isothermal biomass particles, and include external and internal heat transfer [17]. A non-isothermal model has been developed to estimate the yields of volatiles and char at different heating rates, high temperatures (up to 1500°C) and is valid for different biomass particle sizes. The particle model was validated against data from separate pyrolysis experiments performed at an intermediate heating rate (10-$10^3\,\mathrm{K\ s^{-1}}$) in the wire mesh reactor (WMR) and at a high heating rate of ($10^4\,\mathrm{K\ s^{-1}}$) in the drop tube reactor (DTF) [43]. A particle enters a hot gas stream and is heated up by convection and radiation. The unsteady heat conduction equation (Fourier's Law) in cylindrical coordinates (f=1) is used:

$$c_{p,s} \cdot \frac{dT_p}{dt} = \frac{1}{\rho_s} \cdot \frac{1}{r^f} \cdot \frac{\partial}{\partial r} \left(r^f \lambda_{eff} \frac{\partial T_p}{\partial r} \right) \tag{14}$$

The parameters in equation 14 are defined in nomenclature. The effective thermal conductivity (λ_{eff}) inside the particle is approximated by Bellais

and Grønli [41, 42]. A biomass particle can be represented as a plate, a cylinder and a sphere in planar (f=0), cylindrical (f=1), and spherical (f=2) coordinates under the assumption of similar volume to surface ratios using a different characteristic length:

$$d_p = x_{Ma\,min} \qquad (cylinder) \tag{15}$$

$$d_p = \frac{1}{2} \cdot x_{Ma\,min} \quad (plate) \tag{16}$$

$$d_p = \frac{3}{2} \cdot x_{Ma\,min} \quad (sphere) \tag{17}$$

As it has been shown in this work, biomass particles possess large aspect ratios so that a spherical representation should be avoided. A cylindrical shape allows treatment of biomass particles as one-dimensional [9]. Thus, it is recommended to represent biomass particles as infinite cylinders, corresponding to f=1 with a particle size equal to $x_{Ma\,min}$, as shown in equation 15.

Figure 7 illustrates the mass loss of 0.2 and 1 mm pulverized wood particles. The previous results from the 1D model emphasized a key role of intra-particle heat conduction in biomass particle > 0.25 mm [43]. Devolatilization time decreased with the higher heating rate in the drop tube reactor compared to the wire mesh reactor. The representation of the 0.2 mm particles using different characteristics lengths does not give large deviations with respect to char yield and devolatilization time among the three particle geometries as shown in Figure 7(a).

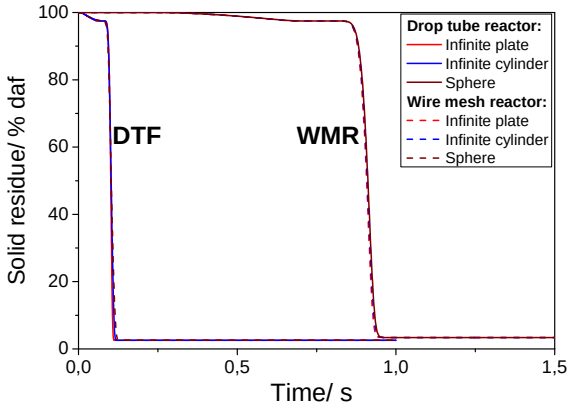

7(a): Pulverized wood 0.2 mm

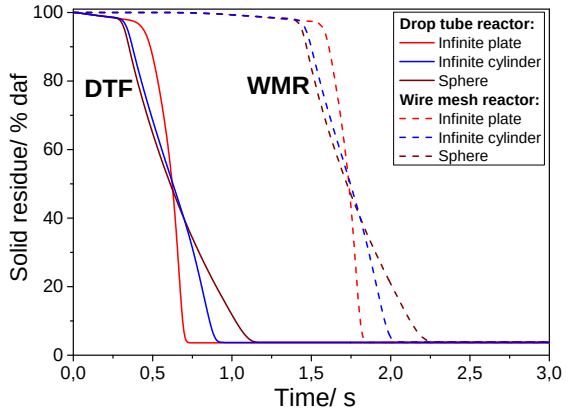

7(b): Pulverized wood 1 mm

Figure 7: Mass loss histories of pulverized wood particles (0.2 and 1 mm) with the similar volume to surface ratio and different characteristic lengths which were calculated in plate-like (n=0), cylindrical (n=1) and spherical (n=2) geometries at the final temperature of 1400°C during pyrolysis in the wire mesh and drop tube reactors.

356 The influence of particle shape becomes more important with the in-

creasing particle size due to the larger internal temperature gradients as shown in Figure 7(b). The relative influence of heating rate on devolatilization time of 1 mm pulverized wood was less as compared to that for smaller particles. This is because of the predominance of internal heat transfer control within the large particles.

3.4. Discussion

Prior to combustion modeling, biomass samples are usually analyzed to obtain the shape parameters (i.e. the sphericity, symmetry and aspect ratio) by using one of the discussed techniques. Various biomass shapes result in different volume-to-surface area ratios which determine heat and mass transfer [9, 44]. A spherical particle, as commonly used in literature [45], has a higher volume to surface area ratio than a cylindrical particle of the same volume. Therefore, particles with a smaller aspect ratio heat up faster, which results in a faster conversion rate. The experimental investigations showed significantly smaller aspect ratios of biomass particles compared to coal, indicating that the spherical representation of a biomass particle (larger volume-to-surface area ratios) overestimates devolatilization time, for example.

Lu et al. [9, 46] measured and calculated particle surface area and volume using a three-dimensional particle shape reconstruction algorithm based on three images taken from orthogonal directions. The particle surface and volume calculation involved image acquisition and processing, image contour alignment and surface generation. In the present study, particle size distributions obtained by 2D dynamic imaging were used to calculate the volume to surface ratio, where $x_{Ma\,min}$ diameter was used as the particle width. The

$x_{Ma\,min}$ diameter can be replaced by $x_{c\,min}$ when a 2D dynamic imaging device is not available, since only small differences occur while representing particle size distributions, based on volume, over $x_{Ma\,min}$ and $x_{c\,min}$ diameters. Alternatively, the average specific surface area can be measured by 2D dynamic imaging, and multiplied by the $\cos(45°)$ factor.

In particle technology, a particle is often represented as an ellipsoid, based on favorable properties such as geometric interlocking and an accurate description of convex particle shapes [47]. In addition, an ellipsoid resembles a large array of shapes, including that of a flake like particle (oblate ellipsoid) and a rod-like particle (prolate ellipsoid) [11]. In the mathematical combustion model, a complete char burnout is a common assumption, so that a rectangular shape can be chosen as the best particle shape descriptor since the rectangular-shaped particles demonstrate the longest burnout times. However, the ellipsoidal and rectangular representations are very difficult to model. The cylindrical representation may give a precise description of char burnout, although the particle volume, compared to the ellipsoidal volume, with equal dimensions tends to be overestimated by the minimal time required for the mass and heat transfer calculations. Moreover, the cylindrical representation does not consider the biomass particles' edges, which influence the heat and mass transfer calculation in combustion modeling.

4. Conclusion

An experimental study was carried out to investigate the particle size and shape characteristics of woody and herbaceous biomass. The particle size results obtained by 2D dynamic imaging were in agreement with the

sieving data. A significant disparity was observed in the laser diffraction and the focused beam reflectance measurements. 2D dynamic imaging was found to be the most convenient characterization method, providing additional information on particle shape and external surface area. Light microscopy and 2D dynamic imaging showed that pulverized wood formed square-shaped particles, while the poplar and wheat straw particles were elongated and of rectangular-shape. It is recommended to represent biomass particles in combustion models as infinite cylinders, where the particle width is represented either by $x_{Ma\,min}$ or $x_{c\,min}$ diameters. The relative influence of heating rate on devolatilization time of larger wood particles was less as compared to that for smaller particles, whereas the influence of particle shape became more important with the increasing particle size due to the predominance of internal heat transfer control within the large particles.

Acknowledgements

The authors would like to acknowledge the financial support received from the Danish Strategic Research Council (Grant Nr. DSF-10-093956), Kempestiftelse, DONG Energy, Vattenfall and HOFOR. We would like also to thank Ian Haley and Brian O'Sullivan from Mettler Toledo for assisting with FBRM measurements. The authors thank DTU Combustion and Harmful Emission Control group for the fruitful discussions. Erika Christ are acknowledged for the article proof reading.

References

[1] Saleh SB, Hansen BB, Jensen PA, Dam-Johansen K, Influence of Biomass Chemical Properties on Torrefication Characteristics, Energy Fuels 27 (2013) 7541–8.

[2] Spinelli R, Cavallo E, Facello A, Magagnotti N, Nati C, Paletto G, Performance and energy efficiency of alternative comminution principles: Chipping versus grinding, Scan J Forest Research 27 (2012) 393–400.

[3] Mandø M, Rosendahl L, Yin C, Sørensen H, Pulverized straw combustion in a low NO_x multifuel burner: Modeling the transition from coal to straw, Fuel 89 (2010) 3051–62.

[4] Abbas T, Costen PG, Lockwood FC, Solid fuel utilization: from coal to biomass, Proc 26th Int Symp Comb (1996) 3041–58.

[5] Tamura M, Watanabe S, Kotake N, Hasegawa M, Grinding and combustion characteristics of woody biomass for co-firing with coal in pulverised coal boilers, Fuel 134 (2014) 544–53.

[6] Rosendahl L, Using a multi-parameter particle shape description to predict the motion of non-spherical particle shape in swirling flow, Appl Math Model 24 (2000) 11–25.

[7] Thunman H, Leckner B, Niklasson F, Johnsson F, Combustion of wood particles - a particle model for eulerian calculations, Combust Flame 129 (2002) 30–46.

[8] Saastamoinen J, Aho M, Moilanen A, Sørensen LH, Clausen S, Berg M, Burnout of pulverized biomass particles in large scale boiler - Single particle model approach, Biomass Bioenergy 34 (2010) 728–36.

[9] Lu H, Ip E, Scott J, Foster P, Vickers M, Baxter LL, Effect of particle shape and size on devolatilization of biomass particles, Fuel 89 (2010) 1156–68.

[10] Ma L, Jones JM, Pourkashanian M, Williams A, Modelling the combustion of pulverized biomass in an industrial combustion test furnace, Fuel 86 (2007) 1959–65.

[11] Mandø M, Turbulence Modulation by Non-Spherical Particles. PhD thesis, Aalborg University (2009).

[12] German RM, Powder Metal Science, Metal Powder Industries Federation, 1984.

[13] Yin C, Rosendahl L, Condra TJ, Use of numerical modeling in design for co-firing biomass in wall-fired burners, Chem Eng Sci 59 (2004) 3281–92.

[14] Yang YB, Sharifi VN, Swithenbank J, Williams A, Combustion of a Single Particle of Biomass, Chemosphere 42 (2001) 481–90.

[15] Sannigrahi P, Ragauskas AJ, Tuskan GA, Poplar as a feedstock for biofuels: A review of compositional characteristics, Biofuels Bioprod Bioref 4 (2010) 209–26.

[16] Trubetskaya A, Jensen PA, Jensen AD, Steibel M, Spliethoff H, Glarborg P, Influence of fast pyrolysis conditions on yield and structural

transformation of biomass char, Fuel Process Technol 140 (2015) 205–14.

[17] Trubetskaya A, Fast pyrolysis of biomass at high temperatures. PhD thesis, Technical University of Denmark (2016).

[18] Stiess M, Mechanische Verfahrenstechnik 1 (in German), Springer, 1992.

[19] Merkus HG, Particle Size Measurements, Springer, 2009.

[20] Saad ES, Mostafa ME, Analysis of Grain Size Statistic and Particle Size Distribution, Waste Biomass Valor 5 (2014) 1005–18.

[21] Williams O, Newbolt G, Eastwick C, Kingman S, Giddings D, Lester E et al., Influence of mill type on densified biomass comminution, Applied Energy 182 (2016) 219–31.

[22] Tannous K, Lam PS, Sokhansanj S, Grace JR, Physical properties for flow characterization of ground biomass from Douglas Fir Wood, Part Sci Technol 31 (2012) 291–300.

[23] Gavlighi HA, Meyer AS, Zaidel DNA, Mohammadifar MA, Mikkelsen JD, Stabilization of emulsions by gum tragacanth (*Astragalus* spp.) correlates to the galacturonic acid content and methoxylation degree of the gum, Food Hydro 31 (2013) 5–14.

[24] Maass S, Wollny S, Voigt A, Kraume M, Experimental comparison of measurement techniques for drop size distribution in liquid/liquid dispersions, Experiments Fluids 50 (2) (2011) 259–69.

[25] Leyssens T, Baudry C, Escudero Hernandez ML, Optimization of Crystallization by Online FBRM Analysis of Needle-Shaped Crystals, Org Process Res 15 (2) (2011) 413–26.

[26] Clain P, Ndoye FT, Delahaye A, Fournaison L, Lin W, Dalmazzone D, Particle size distribution of TBPB hydrates by focused beam reflectance measurement (FBRM) for secondary refrigeration application, Int J Refrige 50 (2015) 19–31.

[27] Heath AR, Fawell PD, Bahri PA, Swift JD, Estimating Average Particle Size by Focused Beam Reflectance Measurement (FBRM), Part Part Syst Charact 19 (2002) 84–95.

[28] Schümann H, Tutkun M, Nydal OJ, Experimental study of dispersed oil-water flow in a horizontal pipe with enhanced inlet mixing, Part 2: In-situ droplet measurements, J Petrol Sci Eng 145 (2016) 753–62.

[29] Trubetskaya A, Poyraz Y, Weber R, Wadenbäck J, Secondary comminution of wood pellets in power plant and laboratory-scale mills, Fuel Process Tech 160 (2017) 216–27.

[30] Gil M, Teruel E, Arauzo I, Analysis of standard sieving method for milled biomass through image processing. Effects of particle shape and size for poplar and corn stover, Fuel 116 (2014) 328–40.

[31] Dhir RK, McCarthy MJ, Concrete durability and repair technology, Thomas Telford, 1999.

[32] Kelly RN, Di Sante KJ, Stranzl E, Kazanjian JA, Bowen P, Matsuyama T et al., Graphical comparison of image analysis and laser diffraction

particle size analysis data obtained from the measurements of non-spherical particle systems, AAPD PharSciTech 7 (3) (2006) 93–106.

[33] Matsuyama T, Yamamoto H, Scarlett B, Theoretical prediction of effect of orientation on diffraction pattern transformation of diffraction pattern due to ellipsoids into equivalent diameter distribution for spheres, Part Part Syst Charact 17 (2000) 41–6.

[34] Umhauer H, Bottlinger M, Effect of particle shape and structure on the results of single particle light-scattering size analysis, Appl Opt 30 (1991) 4980–6.

[35] Doroodchi E, Zulfiqar H, Moghtaderi B, A combined experimental and theoretical study on laboratory-scale comminution of coal and biomass blends, Powder Tech 235 (2013) 412–21.

[36] Eshel G, Levy GJ, Mingelgrin U, Singer MJ, Critical Evaluation of the Use of Laser Diffraction for Particle-Size Distribution Analysis, Soil Sci Soc Am J 68 (2004) 736–43.

[37] Cardoso CR, Oliveira TJP, Santana Junior JA, Ataide CH, Physical characterization of sweet sorghum bagasse, tobacco residue, soy hull and fiber sorghum bagasse particles: Density, particle size and shape distributions, Powder Tech 245 (2013) 105–14.

[38] Igathinathane C, Pordesimo LO, Columbus EP, Batchelor WD, Methuku SR, Shape identification and particle size distribution from basic shape parameters using ImageJ, Comp Electr Agricult 63 (2008) 168–82.

[39] Geimer RL, Evans JW, Setiabudi D, Flake Furnish Characterization: Modeling Board Properties with Geometric Descriptors, Forest Prod Lab, 1999.

[40] Momeni M, Fundamental Study of Single Biomass Particle Combustion. PhD thesis, Aalborg University (2012).

[41] Bellais M, Modelling of the pyrolysis of large wood particles. PhD thesis, KTH Royal Institute of Technology (2007).

[42] Grønli MG, A Theoretical and Experimental Study of the Thermal Degradation of Biomass. PhD thesis, Norwegian University of Science and Technology (1996).

[43] Trubetskaya A, Surup G, Shapiro A, Bates RB, Modeling the influence of potassium content and heating rate on biomass pyrolysis, Appl Energy 194 (2017) 199–211.

[44] Momeni M, Yin C, Kœr SK, Hansen TB, Jensen PA, Glarborg P, Experimental Study on Effects of Particle Shape and Operating Conditions on Combustion Characteristics of Single Biomass Particles, Energy Fuels 27 (2012) 507–14.

[45] Grammelis P, Solid Biofuels for Energy. A Lower Greenhouse Gas Alternative, Springer, 2011.

[46] Lu H, Experimental and modeling investigations of biomass particle combustion. PhD thesis, Brigham Young University (2006).

[47] Hudson PK, Gibson ER, Young MA, Kleiber PD, Grassian VH, Coupled infrared extinction and size distribution measurements for several clay components of mineral dust aerosol, J Geophys Research 113 (2008) 1–11.